ACS APPLIED MATERIALS & INTERFACES

Research Article

www.acsami.org

Fabricating a Cycloolefin Polymer Immunoassay Platform with a Dual-Function Polymer Brush via a Surface-Initiated Photoiniferter-Mediated Polymerization Strategy

Jiao Ma,[†,‡] Shifang Luan,*[,†] Lingjie Song,[†,‡] Jing Jin,[†] Shuaishuai Yuan,[†,‡] Shunjie Yan,[†,§] Huawei Yang,[†] Hengchong Shi,[†] and Jinghua Yin*[,†]

[†]State Key Laboratory of Polymer and Chemistry, Changchun Institute of Applied Chemistry, Chinese Academy of Sciences, Changchun 130022, People's Republic of China

[‡]University of Chinese Academy of Sciences, Beijing 100049, People's Republic of China

[§]Department of Polymer, School of Chemistry and Chemical Engineering, Yantai University, Yantai, 264005, People's Republic of China

Supporting Information

ABSTRACT: The development of technologies for a biomedical detection platform is critical to meet the global challenges of various disease diagnoses. In this study, an inert cycloolefin polymer (COP) support was modified with two-layer polymer brushes possessing dual functions, i.e., a low fouling poly[poly(ethylene glycol) methacrylate] [p-(PEGMA)] bottom layer and a poly(acrylic acid) (PAA) upper layer for antibody loading, via a surface-initiated photoiniferter-mediated polymerization strategy for fluorescence-based immunoassay. It was demonstrated through a confocal laser scanner that, for the as-prepared COP-*g*-PEG-*b*-PAA-IgG supports, nonspecific protein adsorption was suppressed, and the resistance to nonspecific protein interference on antigen recognition was significantly improved, relative to the COP-*g*-PAA-IgG references. This strategy for surface modification of a polymeric platform is also applicable to the fabrication of other biosensors.

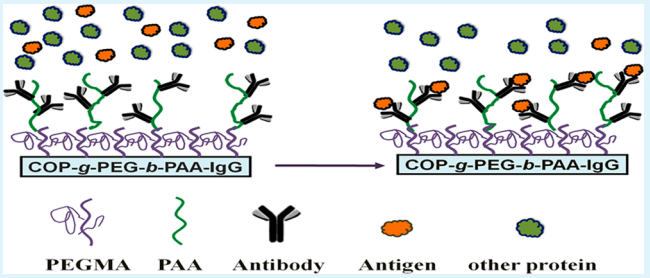

KEYWORDS: *cycloolefin polymer (COP), surface-initiated photoiniferter-mediated polymerization (SI-PIMP), hierarchical architecture, antibody immobilization, immunoassay*

INTRODUCTION

Immunoassays have attracted a great deal of attention in past decades in disease detection, environment, and food monitoring because of their quick, accurate, and sensitive detection of targets.[1−6] Several issues, e.g., substrate materials, antibioadhesion performances, and antibody immobilization strategies, are important for sensitive recognition of target biomolecules.[7−10]

Various polymers, such as polystyrene,[11] poly(ethylene terephthalate),[12] polycarbonate,[13] fluoropolymer,[14] and cycloolefin polymer (COP),[15−17] have been used as bioassay substrates because of their advantages over inorganic materials including time savings, low cost, and ease of fabrication.[18] Because of its high transparency, optical clarity, low autofluorescence, absence of UV absorption, and low birefringence, COP is an ideal material for fabricating cheap disposable biosensor platforms in the biomedical diagnostics industry, especially for point-of-care applications.[19−22] However, its strong hydrophobicity will inevitably render serious bioadhesion, thus resulting in strong background noise, even false signals in diagnostics.[23] Zwitterionic materials[24−28] and poly(ethylene glycol) (PEG) derivatives[29−32] are widely used for imparting hydrophilicity to a substrate.[33]

A proper antibody immobilization strategy is vital to the sensitive recognition of target biomolecules.[6] Compared with the physical adsorption approach, covalently immobilizing an antibody on a substrate exhibits much superiority like stability, effectiveness, and ease of repeatability.[34−38] However, directly conjugating an antibody on a substrate can lead to antibody denaturation because of the hydrophobic substrate and decrease the antigen detection efficiency because of steric hindrance.[9] Thus, long and flexible linkers are popularly adopted to immobilize the antibody.[39−41]

Surface graft polymerization is a series of practicable methods for improving the hydrophilicity of the polymer substrate, even providing reactive sites for immobilizing the antibody.[42−45] Recently, a novel surface-initiated photoiniferter-mediated polymerization (SI-PIMP) has been developed.[46−48] It not

Received: November 8, 2013
Accepted: January 14, 2014
Published: January 14, 2014

only inherits the advantages of conventional photopolymerization, e.g., fast reaction rate, simple equipment, and ease of industrialization, but also possesses controlled polymerization nature.[49−51] Relative to surface-initiated atom-transfer radical polymerization, a significant superiority of SI-PIMP is that the reaction is controlled by a UV-light device and does not utilize toxic catalyst complexes.[52] A two-layer zwitterionic architecture on a gold substrate using the SI-PIMP method was proposed for immunoassay by Jiang's group.[53,54]

There are two challenges in clinical immunoassays, i.e., the high false positives arising from nonspecific protein adsorption and the limited sensitivity arising from low antibody loading. In addition, high antibody loading is accompanied by high nonspecific protein adsorption on unprotected substrates in complex media during detection primarily because of the "loose" polymeric structure.[54−57] This inherent contradiction is expected to be solved by constructing a two-layer polymer brush with dual functions on detection supports. Nevertheless, to the best of our knowledge, fabricating a dual-function polymer brush via SI-PIMP on polymeric substrates, i.e., COP, has not yet been studied.

In this work, for the first time, COP supports were functionalized with a two-layer polymer brush, i.e., a poly[poly(ethylene glycol) methacrylate] [p(PEGMA)] bottom layer and a poly(acrylic acid) (PAA) upper layer, via a SI-PIMP strategy. As for this dual-function hierarchical architecture, specific sites for a covalently binding antibody were provided by carboxyl groups in PAA backbones, and nonspecific protein resistance was achieved by hydrophilic p(PEGMA) polymer brushes. Furthermore, the amount of immobilized antibody, antigen detection, and microarray configuration were investigated by a confocal laser scanning microscopy (CLSM).

EXPERIMENTAL SECTION

Materials. Cycloolefin polymer (COP) Zeonex 690R granules and sheets (1 mm thickness, inject molding) were obtained from ZEON Corp.. Poly(ethylene glycol) methacrylate (PEGMA) monomer (M_n = 360) and sodium diethyldithiocarbamate trihydrate (DETC; >99.0%) were purchased from Sigma-Aldrich. 4-(Chloromethyl)benzoyl chloride (CMBC; >98.0%) was obtained from TCI Shanghai. Acrylic acid (AA; >99.5%) was purchased from Acros Organics. Bovine serum albumin (BSA), fibrinogen (FIB), phosphate-buffered solution (PBS; pH = 7.4), and 2-morpholinoethanesulfonic acid (MES; pH = 3.6) were provided by Dingguo Biotechnology. Rhodamine-labeled bovine serum albumin (Rhd-BSA), goat-anti-rabbit immunoglobulin antibody (Go-anti-Ra IgG), Alexa Fluor 555 labeled goat-anti-rabbit immunoglobulin antibody (A555-Go-anti-Ra IgG), fluorescein isothiocyanate labeled rabbit antibody (FITC-Ra IgG), and Alexa Fluor 488 labeled mouse-anti-goat secondary antibody (A488-Mo-anti-Go IgG) were obtained from Beijing Biosynthesis Biotechnology. *N*-Hydroxysuccinimide (NHS) and 1-ethyl-3-(3-dimethylaminopropyl)carbodiimide (EDC) were obtained from Alfa Aesar. PEGMA and AA were passed through an alumina column to remove the inhibitor and were stored at 4 °C for use. Other chemicals were AR grade.

Photoiniferter Immobilization. The virgin COP supports by hot pressing were cleaned and subjected to oxygen plasma (DT-03 plasma apparatus, Suzhou Omega Technology) under the condition of 90 W and 16 Pa for 60 s. Then the pretreated supports were immersed in a freshly distilled ethyl acetate solution of CMBC [10% (v/v)] and pyridine [3% (v/v)] under an anhydrous atmosphere for 24 h. After sonication in ethanol for 10 min and drying under a nitrogen flow, CMBC-immobilized supports were obtained (denoted as COP-CMBC). They were subsequently soaked in an ethanolic solution of DETC [10% (v/v)] at room temperature for 48 h, and the as-prepared supports were denoted as COP-CBDC. Finally, the supports were thoroughly rinsed with ethanol and deionized water, dried with a nitrogen flow, and stored in a dark environment.

SI-PIMP on COP Supports. The PEGMA aqueous solution (10 vol %) was degassed with a nitrogen stream for 30 min, followed by transfer to a quartz tube containing the COP-CBDC samples under a nitrogen atmosphere. Graft photopolymerization was conducted under UV light (high-pressure mercury lamp, 400 W, main wavelength 380 nm) for a desired time to prepare the p(PEGMA)-grafted supports (denoted as COP-*g*-PEG, and the grafting time of the graft layers was labeled as a subscript), followed by rinsing with water for 12 h and drying under vacuum at 30 °C overnight. Similar to the above graft procedure, the COP-*g*-PEG samples were subjected to another graft photopolymerization of AA [aqueous solution, 10% (v/v)], and the as-prepared samples were denoted as COP-*g*-PEG-*b*-PAA (the grafting time of the graft layers was labeled as a subscript).

Primary Antibody Immobilization. Carboxyl groups on the modified COP surface were activated with a 0.1 M MES solution containing 0.4 M EDC and 0.1 M NHS at 4 °C for 2 h. After rinsing with deionized water and drying under a nitrogen stream, the obtained samples (denoted as COP-*g*-PEG-*b*-PAA-Suc) were soaked in a PBS solution of Go-anti-Ra IgG (100 μg/mL) at 4 °C for 15 h, followed by rinsing with a PBS buffer and deionized water to remove the free antibodies and drying with an argon flow. Thus, COP-*g*-PEG-*b*-PAA-IgG samples were obtained.

Primary Antibody Immobilization Evaluation and Antigen Recognition. The antibody-immobilized samples were blocked with a BSA solution (1 mg/mL) at room temperature for 1 h. After washing with PBS and deionized water, they were incubated in a PBS solution containing A488-Mo-anti-Go IgG (50 μg/mL) at 4 °C for 12 h, followed by rinsing, drying, and examination by fluorescence intensity scanning.

For their antigen recognition, the IgG-immobilized surfaces were soaked in a PBS solution containing FITC-Ra IgG antigen (50 μg/mL) and FIB (0-500 μg/mL) at 4 °C for 24 h, and the physisorbed antigen was removed by a PBS solution and ultrapure water. The samples were tested by fluorescence intensity scanning.

Nonspecific Protein Adsorption Test. As for the nonspecific protein adsorption test, the samples were incubated in a PBS solution for 2 h, then soaked in a PBS solution containing Rhd-BSA (200 μg/mL) at 4 °C for 12 h, rinsed, dried, and finally examined by fluorescence intensity scanning.

Microarrays, Their Antibody Immobilization, and Antigen Recognition. The fabrication of microarrays and the following antibody immobilization and antigen recognition were conducted mainly according to the above procedures. Some different detailed procedures were shown as follows. Microarrays were fabricated in a sandwiched system. That is, the COP supports were put on a quartz plate (3 mm thick) and coated with an aqueous solution of monomer; a photomask was placed on the COP surface, followed by covering with another quartz plate. In addition, A555-Go-anti-Ra IgG was adopted in a primary antibody immobilization procedure.

Surface Chemistry Characterization. ATR-FTIR curves of the samples were obtained by Bruker Vertex 70 Fourier transform infrared spectroscopy equipped with an attenuated total reflection (ATR) unit (crystal 45°) at a resolution of 4 cm^{-1} for 32 scans. The surface composition of the samples was determined via X-ray photoelectron spectroscopy (XPS; VG Scientific ESCA MK II Thermo Avantage V 3.20 analyzer) with an Al Kα ($h\nu$ = 1486.6 eV) anode mono-X-ray source at a detection angle of 90°. The spectra were collected over a range of 0−1200 eV, and high-resolution C 1s spectra were collected. The atomic concentrations of the elements were determined by the peak-area ratios.

Surface Morphology. The surface morphology of the samples was examined by atomic force microscopy in contact mode (AFM; SPA300HV with a SPI 3800 controller, Seiko Instruments Industry). The surface morphology and root-mean-square (rms) roughness were provided by AFM analysis.

Surface Wettability. Water contact angles (WCAs) of the samples were measured by a sessile-drop method with a contact-angle goniometer drop-shape analysis (KRÜSS GmbH) at room temper-

Scheme 1. Preparation of a Detection Platform Modified with Two-Layer Polymer Brushes via a Living SI-PIMP Strategy and Its Antibody Immobilization and Antigen Detection

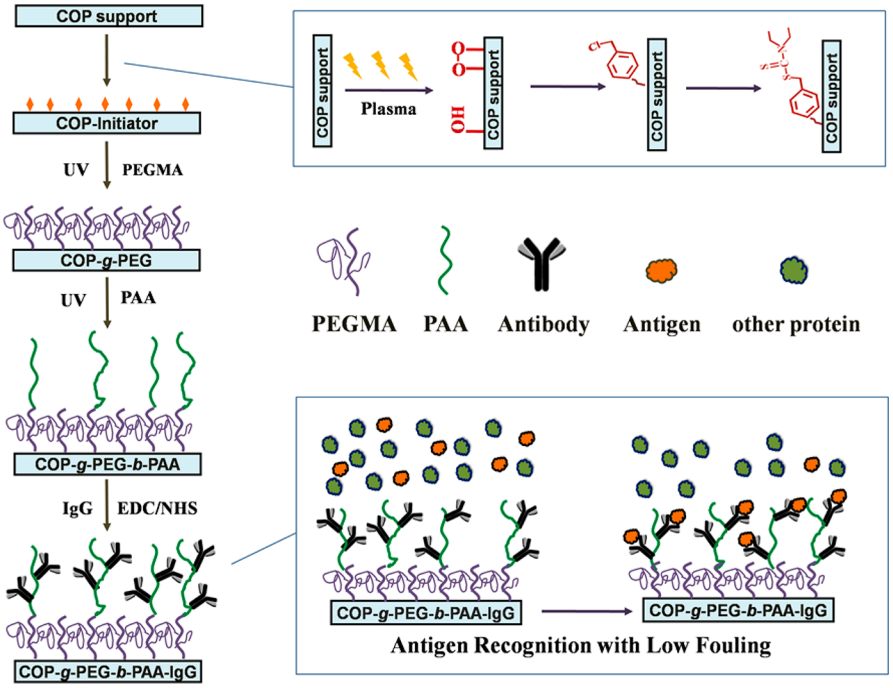

Table 1. Elemental Composition of the COP Supports

	composition (atom %)								
sample	C	N	O	S	Cl	Cl/C (%)	N/C (%)	S/C (%)	O/C (%)
COP	91.44	0.63	7.88	0.06			0.69	0.07	8.61
COP-CMBC	77.27	0.96	20.49	0.18	1.10	1.42	1.24	0.23	26.51
COP-CBDC	86.93	1.36	10.80	0.65	0.27	0.31	1.56	0.75	12.42

ature. For each sample, at least three measurements were performed for calculating the average WCA values.

Fluorescence Intensity Scanning and Data Analysis. Fluorescent images of the samples were collected by a confocal laser scanning microscope (Zeiss, LSM 700).[58,59] Target biomolecules labeled with FITC, Rhd, and Alex Fluor 488 and 555 were respectively excited by an argon-ion laser at 488 and 555 nm. In order to obtain the fluorescence intensity, the original fluorescent images were analyzed using *Image Pro* software from the original images without further treatment.[12,23] The detailed procedures were described as follows. The image was converted into grayscale without affecting the intensity information. After the intensity of each pixel was accumulated, the fluorescence intensity of the whole image was calculated. The fluorescence intensity distribution curves were generated automatically along with the fluorescence images during microscope scanning. This presented the occurrence frequency (y value in the plot) of pixels for a certain fluorescence intensity (x value in the plot) because the fluorescent image actually consists of a lot of pixels with different intensities.

RESULTS AND DISCUSSION

As illustrated in Scheme 1, the inert COP supports were activated by oxygen plasma to form active species such as hydroxyl, carboxyl, and peroxide groups, followed by immobilization of the initiator. Through the SI-PIMP approach, the COP supports were grafted with a PEG-*b*-PAA dual-function polymer brush and utilized for immunoassay.

Surface Characterization. The XPS elemental composition of the COP supports is shown in Table 1. The Cl/C and O/C values increased to 1.42% and 26.51% with the introduction of CMBC and then decreased to 0.31% and 12.42% as chloromethyl reacted with DETC. Correspondingly, the S/C and N/C values respectively rose to 0.75% and 1.56% because of the −S−C═S−N structure. These changes confirmed the successful introduction of the initiator. SI-PIMP of PEGMA and AA onto the initiator-modified supports was sequentially conducted. In ATR-FTIR spectra of these samples provided in Figure 1, two new adsorption peaks at 1730 cm^{-1} (C═O, stretching vibration) and 1137 cm^{-1} (C−

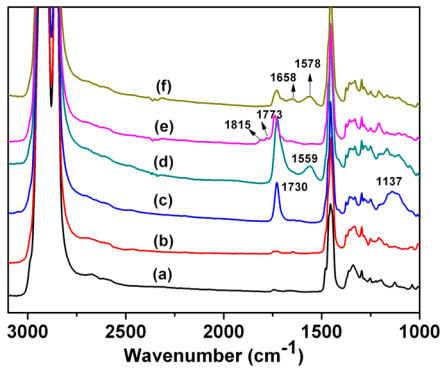

Figure 1. ATR-FTIR spectra of the COP supports: (a) virgin COP; (b) COP-CBDC; (c) COP-*g*-$PEG_{12\ min}$; (d) COP-*g*-$PEG_{12\ min}$-*b*-$PAA_{8\ min}$; (e) COP-*g*-$PEG_{12\ min}$-*b*-$PAA_{8\ min}$-Suc; (f) COP-*g*-$PEG_{12\ min}$-*b*-$PAA_{8\ min}$-IgG.

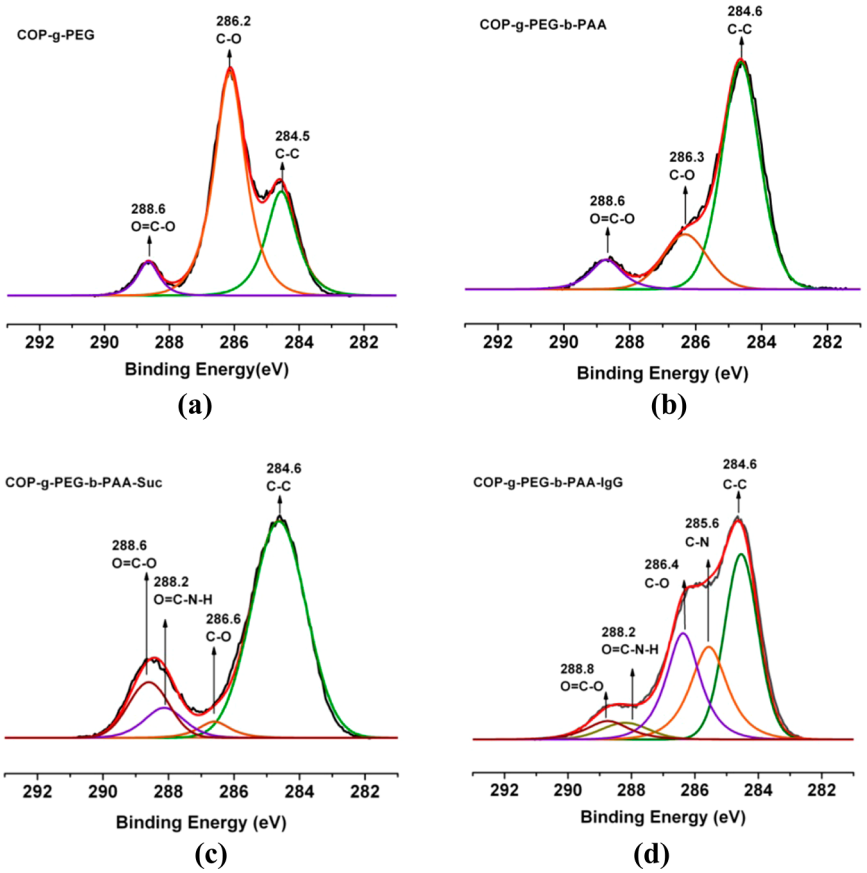

Figure 2. High-resolution XPS C 1s spectra and their peak fitting curves of the samples: (a) COP-*g*-PEG; (b) COP-*g*-PEG-*b*-PAA; (c) COP-*g*-PEG-*b*-PAA-Suc; (d) COP-*g*-PEG-*b*-PAA-IgG.

O−C, stretching vibration) were observed on the p(PEGMA)-modified supports. After grafting with AA, a new peak attributed to carboxyl groups (at 1559 cm^{-1}) appeared. In addition, two peaks at 1815 and 1773 cm^{-1} belonging to the succinimidyl ester structure demonstrated the EDC/NHS activation of carboxyl groups. The amide I and amide II structures (at about 1658 and 1578 cm^{-1}) emerged with the introduction of IgG.

To fully distinguish the functional groups on the polymer brush-modified supports, their high-resolution C 1s spectra and peak-fitting curves were used and are given in Figure 2. In detail, the C 1s spectra of the COP-*g*-PEG samples were decomposed into three peaks: a *C*−H (*C*−C) peak at 284.5 eV, a C−O peak at 286.2 eV, and a O═*C*−O peak at 288.6 eV, respectively. TheC−O peak mainly attributed to polyether structures diminished because of the additional introduction of a PAA layer, and a new O═*C*−N−H peak at 288.2 eV and a new *C*−N peak at 285.6 eV were found respectively on the COP-*g*-PEG-*b*-PAA-Suc and COP-*g*-PEG-*b*-PAA-IgG samples.

In order to investigate the controlled polymerization nature of SI-PIMP on COP supports, we used origin software to integrate the area of peak at 1728 cm^{-1} attributed to the O═C−O groups in p(PEGMA) graft chains and the total area of two peaks at 2923 and 2854 cm^{-1} mostly belonging to C−H groups in COP chains (Figure 3a). The obtained area ratio R ($A_{1728}/A_{2854,\ 2923}$) represented the percentage of the p(PEGMA) layer in the matrix.[57,60] It was found that R value rose linearly as the SI-PIMP time elapsed (Figure 3b). These results were consistent with the previous work,[61,62] in which a controlled graft process was demonstrated by the linear growth of the graft layer thickness with graft time. Thus, we can conclude that the polymer brush growing from the COP-CBDC surface is conducted in a "controlled" manner.

Topography changes on COP supports were studied using AFM and are shown in Figure 4. Low rms roughness values, i.e., 3.07, 3.25, and 4.78 nm, were observed on COP, COP-CBDC, and COP-*g*-PEG surfaces, suggesting that uniform polymer brushes were prepared by the controlled SI-PIMP technique. SI-PIMP is apt to release capped species from the polymer chains during polymerization, primarily because of bimolecular termination (i.e., chain−chain radical recombination). This irreversible termination renders the loss of some initiated sites, leading to the formation of an upper graft layer with a low surface packing density.[53] Thus, a hierarchical architecture consisting of PEG and PAA layers could be confirmed based on the results of increasing rms roughness (8.43 nm) on the surface of COP-*g*-PEG-*b*-PAA. Most recently, the stratified polymer grafts through a sequential SI-PIMP approach have also been verified by a combination of AFM-based nanomechanical testing and lateral force microscopy.[63]

Nonspecific Protein Adsorption. Herein, the samples were immersed in a Rhd-BSA solution, followed by recording of their fluorescence images (Figure S2 in the Supporting Information, SI) and analysis of the amount of nonspecific adsorbed protein (Figure 5). A direct visual comparison of these images confirmed that the COP-*g*-$PEG_{12\ min}$ surfaces (a WCA of 60° in Figure S1 in the SI) suppressed protein adsorption compared with the virgin COP (a WCA of 100° in Figure S1 in the SI) and COP-CBDC (a WCA of 78° in Figure S1 in the SI) supports (Figure S2 in the SI). Quantitative

dx.doi.org/10.1021/am405017h | ACS Appl. Mater. Interfaces 2014, 6, 1971−1978

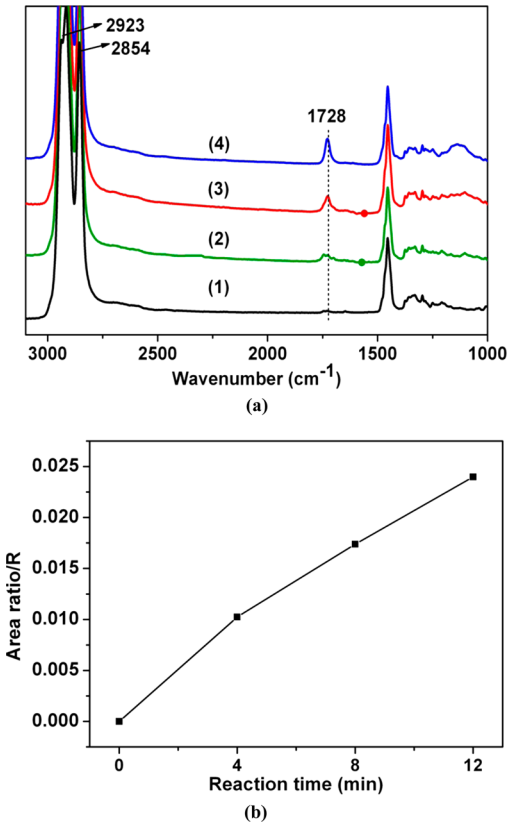

Figure 3. ATR-FTIR spectra (a) and the relationship between the area ratio ($R = A_{1728}/A_{2854,\ 2923}$) and the grafting time (b) of the samples: (1) COP-CBDC; (2) COP-*g*-PEG$_{4\ min}$; (3) COP-*g*-PEG$_{8\ min}$; (4) COP-*g*-PEG$_{12\ min}$.

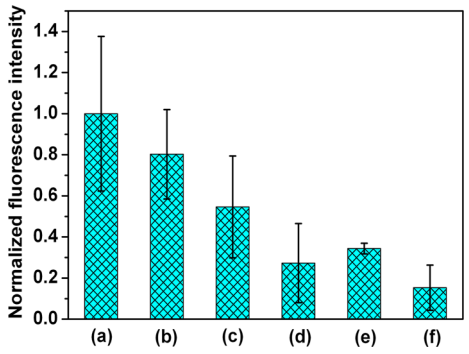

Figure 5. Adsorption of Rhd-BSA on the samples: (a) virgin COP; (b) COP-CBDC; (c) COP-*g*-PEG$_{6\ min}$; (d) COP-*g*-PEG$_{12\ min}$; (e) COP-*g*-PEG$_{12\ min}$-*b*-PAA$_{8\ min}$; (f) COP-*g*-PEG$_{12\ min}$-*b*-PAA$_{8\ min}$-IgG (error bars: standard deviations, $n = 3$).

analysis of these images demonstrated that the amount of protein adsorption respectively decreased by 20%, 46%, and 73% on COP-CBDC, COP-*g*-PEG$_{6\ min}$, and COP-*g*-PEG$_{12\ min}$ samples, relative to that on virgin COP supports. After the additional introduction of PAA (a WCA of 40° in Figure S1 in the SI) and antibody (a WCA of 55° in Figure S1 in the SI), no significant difference for the amount of protein adsorption was observed.

Primary Antibody Immobilization Evaluation and Antigen Recognition. For evaluation the immunoassay performance of this COP platform with a PEG-*b*-PAA hierarchical architecture, we compared it with COP and COP-*g*-PAA supports. Antibodies were physically adsorbed on the virgin COP supports primarily driven by hydrophobic interactions between antibodies and supports. In contrast, antibodies were covalently immobilized on COP-*g*-PAA and COP-*g*-PEG-*b*-PAA supports by using the EDC/NHS coupling

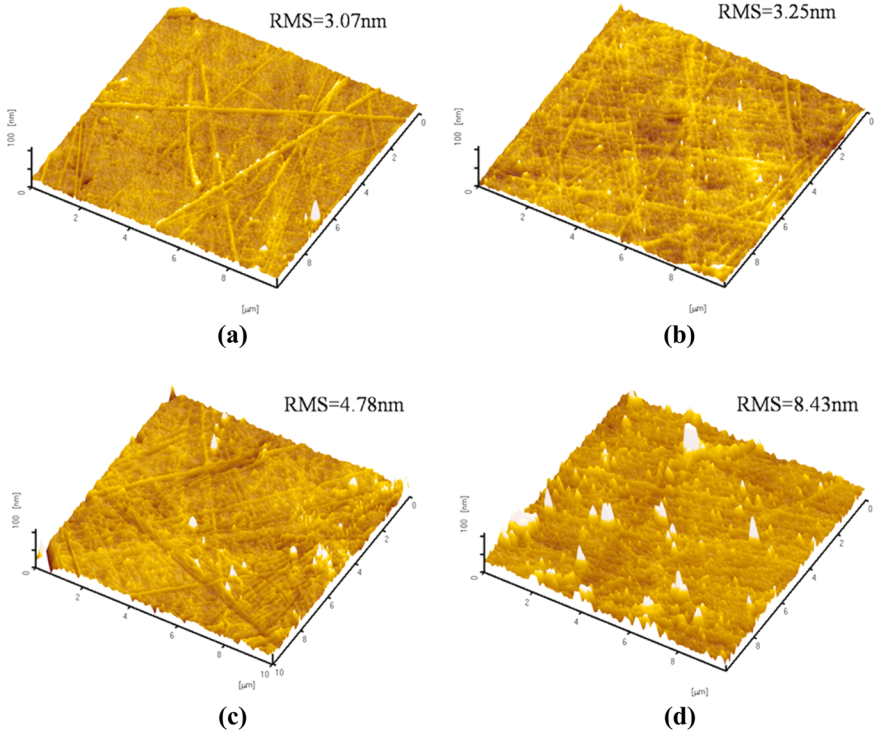

Figure 4. AFM three-dimensional images of the samples: (a) virgin COP; (b) COP-CBDC; (c) COP-*g*-PEG$_{12\ min}$; (d) COP-*g*-PEG$_{12\ min}$-*b*-PAA$_{8\ min}$.

dx.doi.org/10.1021/am405017h | ACS Appl. Mater. Interfaces 2014, 6, 1971−1978

chemistry. Despite many drawbacks of the physical adsorption approach, it has been used in many fields such as ELISA, immunosensors, and antibody arrays, principally because of its high antibody-binding capacity.[9] Notably, the amounts of covalently immobilized antibodies on the surfaces of COP-*g*-PAA and COP-*g*-PEG-*b*-PAA were nearly twice as high as that of the COP surface via physical adsorption (Figures 6a and S3 in the SI). In addition, for COP-*g*-PEG-*b*-PAA-IgG supports, a three-dimensional space distribution of antibodies in a polymer brush facilitated the collision between antibodies and free antigens. The antigen detection amount on the surface of COP-*g*-PEG-*b*-PAA-IgG supports improved a lot compared with that of the COP samples (Figures 6a and S3 in the SI). Thus, the antigen detection efficiency was significantly improved. Furthermore, fluorescence intensity distribution curves also supported the above results from another perspective (Figure 6b,c).

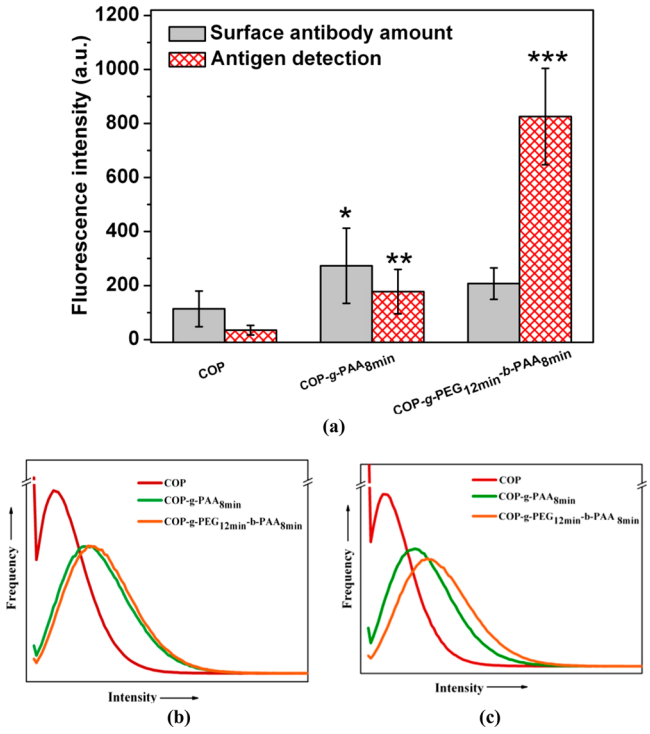

Figure 6. Amount of antibody immobilization and antigen recognition (a). Data were analyzed using a one-way *ANOVA*: *, $p < 0.05$; **, $p < 0.01$; ***, $p < 0.001$. There were significant differences from the prior sample in this picture. Fluorescence intensity distribution curves for antibody immobilization evaluation (b) and antigen recognition (c) (error bars: standard deviations, $n = 3$).

Although antibody-binding capacities on these supports had no significant difference, antigen detection on the surfaces of COP-*g*-PEG-*b*-PAA-IgG and COP-*g*-PAA-IgG showed evident differences. The fluorescence intensity for antigen detection on the surface of COP-*g*-PEG-*b*-PAA-IgG was 5-fold for that of the COP-*g*-PAA-IgG surface (Figures 6a and S3 in the SI). It could be generally attributed to the following reasons. First, a highly dense p(PEGMA) hydrated bottom layer in the hierarchical architecture prevented the immobolized antibodies from strongly hydrophobically interacting with a native COP substrate. The loss of bioactivity of the antibody was inhibited, therefore contributing to the following antigen detection. Second, the existence of flexible p(PEGMA) spacers could strengthen free movement of antibodies on the PAA grafts, which also promoted antigen recognition.[55,64]

Furthermore, fluorescent images of polymer brush microarrays with antibody and target antigen are provided in Figure 7. For PAA and PEG-*b*-PAA brushes, no clear fluorescence was observed under excitement (Figure 7a-1,a-2). The uniform and strong red fluorescence across microarray regions suggested that considerable amounts of IgG have bound successfully to the microdomains (Figure 7b-1,b-2). After specifically interacting with target antigen, the uniform and strong green fluorescence microarray images were still observed on the COP-*g*-PEG-*b*-PAA-IgG support, in contrast to the weak fluorescence images on the COP-*g*-PAA-IgG reference. These results confirmed that not only did the immobilized antibody specifically recognize its target antigen but also the COP-*g*-PEG-*b*-PAA-IgG support had a better capability of antigen recognition relative to the COP-*g*-PAA-IgG reference. The present approach could also be used for biomedical applications including lab-on-chip devices, bio-MEMs, and biosensors.[65]

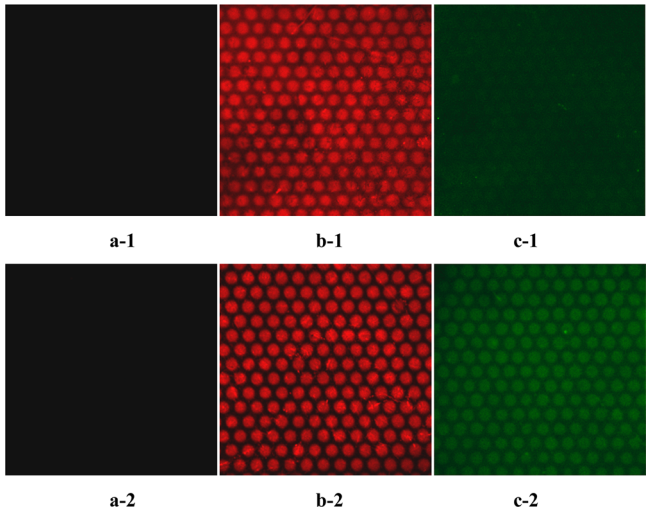

Figure 7. Fluorescent images of polymer brush microarrays (a), antibody-immobilized microarrays (b), and microarrays with target antigen (c): (1) COP-*g*-$PAA_{8\ min}$; (2) COP-*g*-$PEG_{12\ min}$-*b*-$PAA_{8\ min}$. Picture area: 639.5 μm × 639.5 μm.

Effect of Nonspecific Protein Interference on Antigen Recognition. To detect a specific disease marker in practice, biosensors were usually conducted in complicated crude blood or body fluid media. The undesired nonspecific components seriously hindered and interferred with the specific detection of the analyte. Herein, we selected FIB as a model protein because of its abundance in plasma to explore the effect of nonspecific protein on antigen recognition.[66] The samples were first immersed in a solution containing 50 μg/mL FITC-Ra IgG and FIB (0, 50, 100, 200, and 500 μg/mL), followed by examination with CLSM. The COP-*g*-PAA-IgG samples were chosen as references to evaluate the function of the p(PEGMA) bottom layer on the surface of COP-*g*-PEG-*b*-PAA-IgG .

Combining *Image Pro* with *ANOVA*, we calculated the statistical difference of the fluorescence intensity (Figure 8a). For the COP-*g*-PAA-IgG immunoassay, it presented a statistically significant difference ($p < 0.01$) from the prior FIB concentration (50 μg/mL), suggesting that the antigen recognition capability was greatly weakened at a FIB concentration of 100 μg/mL. Also, the antigen recognition

dx.doi.org/10.1021/am405017h | *ACS Appl. Mater. Interfaces* 2014, 6, 1971−1978

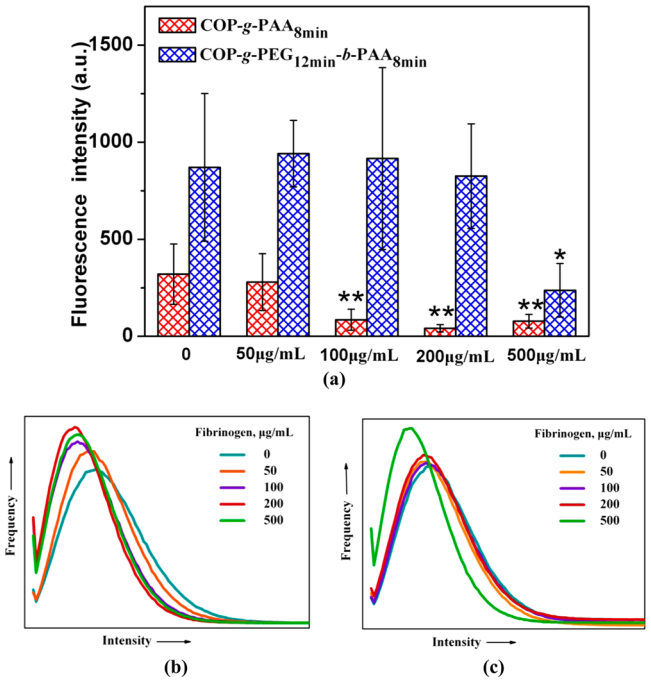

Figure 8. Antigen recognition efficiency (a) and fluorescence intensity distribution curves for the FITC-Ra IgG recognition on the samples of COP-*g*-$PAA_{8\ min}$ (b) and COP-*g*-$PEG_{12\ min}$-*b*-$PAA_{8\ min}$ (c). The experiments were conducted in the 50 μg/mL FITC-Ra IgG solution containing different concentrations of FIB: 0, 50, 100, 200, 500 μg/mL. Data analyzed using a one-way *ANOVA*: *, $p < 0.05$; **, $p < 0.01$; ***, $p < 0.001$. There were significant differences from the prior sample in the picture (error bars: standard deviations, $n = 3$).

capability was significantly suppressed as the FIB concentration further increased. In contrast, the COP-*g*-PEG-*b*-PAA-IgG support presented a similar antigen recognition amount in the presence of FIB with a concentration up to 200 μg/mL, suggesting that COP-*g*-PEG-*b*-PAA-IgG supports exhibited stronger resistance to FIB interference than COP-*g*-PAA-IgG supports. As for fluorescence intensity distribution curves, the curve for COP-*g*-PAA-IgG moved toward a lower intensity direction as the FIB concentration increased (Figure 8b), while there was nearly no movement for COP-*g*-PEG-*b*-PAA-IgG curves until the FIB concentration reached 500 μg/mL (Figure 8c). Both the p(PEGMA) bottom layer and the special hierarchical architecture played important roles in resisting nonspecific protein interference on antigen recognition.

CONCLUSIONS

In this work, we have successfully fabricated a fluorescence-based immunoassay on COP supports via the SI-PIMP strategy. It was demonstrated that a two-layer architecture on COP supports that combined a nonfouling p(PEGMA) bottom layer with a PAA upper layer for antibody loading could improve the antigen detection efficiency and suppress the FIB interference on antigen recognition compared with the COP-*g*-PAA-IgG references. The method for fabricating a polymeric bioassay platform will be diversely applicable to various immunoassays.

ASSOCIATED CONTENT

Supporting Information

WCA values and representative confocal laser microscope images for protein adsorption, antibody immobilization evaluation, and antigen recognition. This material is available free of charge via the Internet at http://pubs.acs.org.

AUTHOR INFORMATION

Corresponding Authors

*E-mail: sfluan@ciac.ac.cn. Tel.: +86 431 85262109. Fax: +86 431 85262109.

*E-mail: yinjh@ciac.ac.cn. Tel.: +86 431 85262109. Fax: +86 431 85262109.

Notes

The authors declare no competing financial interest.

ACKNOWLEDGMENTS

The authors acknowledge financial support of the National Natural Science Foundation of China (Projects 21274150 and 51273200), Chinese Academy of Sciences-Wego Group High-tech Research & Development Program (2011−2013), and Scientific Development Program of Jilin Province (Project 20130102064JC).

REFERENCES

(1) Gubala, V.; Harris, L. F.; Ricco, A. J.; Tan, M. X.; Williams, D. E. *Anal. Chem.* **2012**, *84*, 487−515.
(2) Brault, N. D.; Gao, C.; Xue, H.; Piliarik, M.; Homola, J.; Jiang, S.; Yu, Q. *Biosens. Bioelectron.* **2010**, *25*, 2276−2282.
(3) Zhang, Q. Z.; Zhao, B.; Yan, J.; Song, S. P.; Min, R.; Fan, C. H. *Anal. Chem.* **2011**, *83*, 9191−9196.
(4) Aied, A.; Zheng, Y.; Pandit, A.; Wang, W. X. *ACS Appl. Mater. Interfaces* **2012**, *4*, 826−831.
(5) Liu, G.; Chen, H. D.; Peng, H. Z.; Song, S. P.; Gao, J. M.; Lu, J. X.; Ding, M.; Li, L. Y.; Ren, S. Z.; Zou, Z. Y.; Fan, C. H. *Biosens. Bioelectron.* **2011**, *28*, 308−313.
(6) Gubala, V.; Gandhiraman, R. P.; Volcke, C.; Doyle, C.; Coyle, C.; James, B.; Daniels, S.; Williams, D. E. *Analyst* **2010**, *135*, 1375−1381.
(7) Zhou, F.; Wang, M. M.; Yuan, L.; Cheng, Z. P.; Wu, Z. Q.; Chen, H. *Analyst* **2012**, *137*, 1779−1784.
(8) Song, S. P.; Qin, Y.; He, Y.; Huang, Q.; Fan, C. H.; Chen, H. Y. *Chem. Soc. Rev.* **2010**, *39*, 4234−4243.
(9) Jung, Y. W.; Jeong, J. Y.; Chung, B. H. *Analyst* **2008**, *133*, 697−701.
(10) Zhou, F.; Yuan, L.; Wang, H. W.; Li, D.; Chen, H. *Langmuir* **2011**, *27*, 2155−2158.
(11) Thomson, D. A. C.; Dimitrov, K.; Cooper, M. A. *Analyst* **2011**, *136*, 1599−1607.
(12) Hwang, I.-T.; Kuk, I.-S.; Jung, C.-H.; Choi, J.-H.; Nho, Y.-C.; Lee, Y.-M. *ACS Appl. Mater. Interfaces* **2011**, *3*, 2235−2239.
(13) Yang, D.; Niu, X.; Liu, Y.; Wang, Y.; Gu, X.; Song, L.; Zhao, R.; Ma, L.; Shao, Y.; Jiang, X. *Adv. Mater.* **2008**, *20*, 4770−4775.
(14) Jung, C. H.; Hwang, I. T.; Kuk, I. S.; Choi, J. H.; Oh, B. K.; Lee, Y. M. *ACS Appl. Mater. Interfaces* **2013**, *5*, 2155−2160.
(15) Laib, S.; MacCraith, B. D. *Anal. Chem.* **2007**, *79*, 6264−6270.
(16) Brassard, D.; Clime, L.; Li, K. B.; Geissler, M.; Miville-Godin, C.; Roy, E.; Veres, T. *Lab Chip* **2011**, *11*, 4099−4107.
(17) Diaz-Quijada, G. A.; Peytavi, R.; Nantel, A.; Roy, E.; Bergeron, M. G.; Dumoulin, M. M.; Veres, T. *Lab Chip* **2007**, *7*, 856−862.
(18) Xu, F. J.; Liu, L. Y.; Yang, W. T.; Kang, E. T.; Neoh, K. G. *Biomacromolecules* **2009**, *10*, 1665−1674.
(19) Jonsson, C.; Aronsson, M.; Rundstrom, G.; Pettersson, C.; Mendel-Hartvig, I.; Bakker, J.; Martinsson, E.; Liedberg, B.; MacCraith, B.; Ohman, O.; Melin, J. *Lab Chip* **2008**, *8*, 1191−1197.
(20) Geissler, M.; Roy, E.; Diaz-Quijada, G. A.; Galas, J. C.; Veres, T. *ACS Appl. Mater. Interfaces* **2009**, *1*, 1387−1395.
(21) Roy, E.; Geissler, M.; Galas, J.-C.; Veres, T. *Microfluid. Nanofluid.* **2011**, *11*, 235−244.
(22) Larsson, A.; Ekblad, T.; Andersson, O.; Liedberg, B. *Biomacromolecules* **2007**, *8*, 287−295.

(23) Tajima, N.; Takai, M.; Ishihara, K. *Anal. Chem.* **2011**, *83*, 1969−1976.
(24) Gao, C.; Li, G.; Xue, H.; Yang, W.; Zhang, F.; Jiang, S. *Biomaterials* **2010**, *31*, 1486−1492.
(25) Matsuda, Y.; Kobayashi, M.; Annaka, M.; Ishihara, K.; Takahara, A. *Langmuir* **2008**, *24*, 8772−8778.
(26) Vaisocherová, H.; Zhang, Z.; Yang, W.; Cao, Z.; Cheng, G.; Taylor, A. D.; Piliarik, M.; Homola, J.; Jiang, S. *Biosens. Bioelectron.* **2009**, *24*, 1924−1930.
(27) Zhao, J.; Song, L. J.; Shi, Q.; Luan, S. F.; Yin, J. H. *ACS Appl. Mater. Interfaces* **2013**, *5*, 5260−5268.
(28) Jiang, S.; Cao, Z. *Adv. Mater.* **2010**, *22*, 920−932.
(29) Xiu, K. M.; Cai, Q.; Li, J. S.; Yang, X. P.; Yang, W. T.; Xu, F. J. *Colloids Surf., B* **2012**, *90*, 177−183.
(30) Chen, H.; Wang, L.; Zhang, Y. X.; Li, D.; McClung, W. G.; Brook, M. A.; Sheardown, H.; Brash, J. L. *Macromol. Biosci.* **2008**, *8*, 863−870.
(31) Xu, F. J.; Li, H. Z.; Li, J.; Eric Teo, Y. H.; Zhu, C. X.; Kang, E. T.; Neoh, K. G. *Biosens. Bioelectron.* **2008**, *24*, 773−780.
(32) Yang, H.; Luan, S.; Zhao, J.; Shi, H.; Li, X.; Song, L.; Jin, J.; Shi, Q.; Yin, J.; Shi, D.; Stagnaro, P. *Polymer* **2012**, *53*, 1675−1683.
(33) Yu, Q. A.; Zhang, Y. X.; Wang, H. W.; Brash, J.; Chen, H. *Acta Biomater.* **2011**, *7*, 1550−1557.
(34) Batalla, P.; Fuentes, M.; Mateo, C.; Grazu, V.; Fernandez-Lafuente, R.; Guisan, J. M. *Biomacromolecules* **2008**, *9*, 2230−2236.
(35) Gubala, V.; Le Guevel, X.; Nooney, R.; Williams, D. E.; MacCraith, B. *Talanta* **2010**, *81*, 1833−1839.
(36) Trilling, A. K.; Beekwilder, J.; Zuilhof, H. *Analyst* **2013**, *138*, 1619−1627.
(37) Gubala, V.; Siegrist, J.; Monaghan, R.; O'Reilly, B.; Gandhiraman, R. P.; Daniels, S.; Williams, D. E.; Ducree, J. *Anal. Chim. Acta* **2013**, *760*, 75−82.
(38) Gandhiraman, R. P.; Volcke, C.; Gubala, V.; Doyle, C.; Basabe-Desmonts, L.; Dotzler, C.; Toney, M. F.; Iacono, M.; Nooney, R. I.; Daniels, S.; James, B.; Williams, D. E. *J. Mater. Chem.* **2010**, *20*, 4116−4127.
(39) Raj, J.; Herzog, G.; Manning, M.; Volcke, C.; MacCraith, B. D.; Ballantyne, S.; Thompson, M.; Arrigan, D. W. M. *Biosens. Bioelectron.* **2009**, *24*, 2654−2658.
(40) Trmcic-Cvitas, J.; Hasan, E.; Ramstedt, M.; Li, X.; Cooper, M. A.; Abell, C.; Huck, W. T. S.; Gautrot, J. E. *Biomacromolecules* **2009**, *10*, 2885−2894.
(41) Goto, Y.; Matsuno, R.; Konno, T.; Takai, M.; Ishihara, K. *Biomacromolecules* **2008**, *9*, 828−833.
(42) Edlund, U.; Källrot, M.; Albertsson, A. C. *J. Am. Chem. Soc.* **2005**, *127*, 8865−8871.
(43) Byambaa, B.; Konno, T.; Ishihara, K. *Colloids Surf., B* **2012**, *99*, 1−6.
(44) Xu, Y.; Takai, M.; Ishihara, K. *Biomaterials* **2009**, *30*, 4930−4938.
(45) Vaisocherová, H.; Yaan, W.; Zhang, Z.; Cao, Z.; Cheng, G.; Piliarik, M.; Homola, J. i.; Jiang, S. *Anal. Chem.* **2008**, *80*, 7894−7901.
(46) Benetti, E. M.; Reimhult, E.; de Bruin, J.; Zapotoczny, S.; Textor, M.; Vancso, G. J. *Macromolecules* **2009**, *42*, 1640−1647.
(47) Barbey, R.; Lavanant, L.; Paripovic, D.; Schuwer, N.; Sugnaux, C.; Tugulu, S.; Klok, H. A. *Chem. Rev.* **2009**, *109*, 5437−5527.
(48) Benetti, E. M.; Zapotoczny, S.; Vancso, J. *Adv. Mater.* **2007**, *19*, 268−271.
(49) Edlund, U.; Danmark, S.; Albertsson, A. C. *Biomacromolecules* **2008**, *9*, 901−905.
(50) Luan, S. F.; Zhao, J.; Yang, H. W.; Shi, H. C.; Jin, J.; Li, X. M.; Liu, J. C.; Wang, J. W.; Yin, J. H.; Stagnaro, P. *Colloids Surf., B* **2012**, *93*, 127−134.
(51) Källrot, M.; Edlund, U.; Albertsson, A. C. *Biomaterials* **2006**, *27*, 1788−1796.
(52) Krause, J. E.; Brault, N. D.; Li, Y. T.; Xue, H.; Zhou, Y. B.; Jiang, S. Y. *Macromolecules* **2011**, *44*, 9213−9220.
(53) Huang, C. J.; Brault, N. D.; Li, Y.; Yu, Q.; Jiang, S. *Adv. Mater.* **2012**, *24*, 1834−1837.
(54) Huang, C. J.; Li, Y. T.; Jiang, S. Y. *Anal. Chem.* **2012**, *84*, 3440−3445.
(55) Hu, W.; Liu, Y.; Lu, Z.; Li, C. M. *Adv. Funct. Mater.* **2010**, *20*, 3497−3503.
(56) Iwasaki, Y.; Omichi, Y.; Iwata, R. *Langmuir* **2008**, *24*, 8427−8430.
(57) Larsson, A.; Ekblad, T.; Andersson, O.; Liedberg, B. *Biomacromolecules* **2007**, *8*, 287−295.
(58) Cho, Y.; Cho, D.; Park, J. H.; Frey, M. W.; Ober, C. K.; Joo, Y. L. *Biomacromolecules* **2012**, *13*, 1606−1614.
(59) Goli, K. K.; Rojas, O. J.; Genzer, J. *Biomacromolecules* **2012**, *13*, 3769−3779.
(60) Buck, M. E.; Zhang, J.; Lynn, D. M. *Adv. Mater.* **2007**, *19*, 3951−3955.
(61) Sui, X.; Zapotoczny, S.; Benetti, E. M.; Memesa, M.; Hempenius, M. A.; Vancso, G. J. *Polym. Chem.* **2011**, *2*, 879−884.
(62) Liu, Q.; Singh, A.; Liu, L. *Biomacromolecules* **2012**, *13*, 1086−1092.
(63) Li, A.; Ramakrishna, S. N.; Nalam, P. C.; Benetti, E. M. *Adv. Mater. Interf.* **2013**, DOI: 10.1002/admi.201300007.
(64) Hucknall, A.; Kim, D.-H.; Rangarajan, S.; Hill, R. T.; Reichert, W. M.; Chilkoti, A. *Adv. Mater.* **2009**, *21*, 1968−1971.
(65) Li, C. Y.; Xu, F. J.; Yang, W. T. *Langmuir* **2013**, *29*, 1541−1550.
(66) Martins, M. C. L.; Wang, D.; Ji, J.; Feng, L.; Barbosa, M. A. *Biomaterials* **2003**, *24*, 2067−2076.